JOURNAL OF THERMOPHYSICS AND HEAT TRANSFER
Vol. 25, No. 1, January–March 2011

Performance Model of the Top Filling Configurations for No-Vent Fills

Caili Wang,* Yang Li,† Dong Deng,† Rongshun Wang,‡ and Gaofeng Xie†
Shanghai Jiaotong University, 200240 Shanghai, People's Republic of China

DOI: 10.2514/1.49564

No-vent fill is a promising technology for ground filling applications of dangerous cryogens such as liquefied natural gas and precious liquefied gas such as liquid helium and liquid hydrogen. A finite difference lumped analysis using a Python computer program that predicts no-vent fill performance in a 1 *g* environment for the top filling configurations is described. The tank system is divided into four lumps: the tank wall in contact with the ullage space, tank wall in contact with the bulk liquid, tank wall in contact with the spray incoming liquid, and the cryogen. A new method of dealing with heat transfer between the tank wall and the cryogen is introduced to improve the reliability of the simulation. Corrections of assumptions on the initial distribution of the wall temperature and the inflow rate of the incoming liquid are proposed. Experiments of both the top-spray and the top-nozzle filling configurations are conducted to validate the new model. The results are shown to match the test results within the measurement uncertainty of the test data.

Nomenclature

A_{outlet}	=	outlet area of incoming liquid, m^2
C	=	heat capacity of tank wall, $J/(kg \cdot K)$
D	=	the thickness of the tank wall, m
H	=	liquid level, m
H_s	=	the maximum liquid level to be sprayed on the wall
h	=	enthalpy, J/kg; or heat transfer coefficient, W/m^2 K
h_{fg}	=	latent heat, J/kg
M	=	mass of tank wall, kg
m	=	mass of cryogen, kg
$\dot{m}$	=	mass rate, kg/s
P_{supply}	=	the supply pressure, MPa
Q	=	heat transfer rate, J/kg
T	=	temperature, K
$\bar{T}$	=	average temperature, K
T_{wall}	=	wall temperature, K
t	=	time, s
u	=	internal energy, J/kg
V_{tank}	=	tank volume, m^3
α	=	heat transfer coefficients, W/m^2 K
ΔP	=	pressure difference ($P_{\text{supply}} - P_0$), MPa
γ	=	characteristic coefficient of the fluid transfer pipe
λ_f	=	flashing evaporation coefficient
ρ	=	density, kg/m^3

Subscripts

cw	=	cold wall
cw$l$	=	between cold wall and the liquid bulk
f	=	flashing evaporation
g	=	vapor phase
hw$g$	=	between hot wall and ullage space
in	=	incoming liquid
l	=	liquid phase
old value	=	value at the end of the last time step
sat	=	saturated condition
sw$l$	=	between spray area and incoming liquid
0	=	initial condition

Received 23 February 2010; revision received 31 August 2010; accepted for publication 2 October 2010.

*Ph.D. Graduate Student, Institute of Refrigeration and Cryogenic Engineering, 800 Dongchuan Road; Wangcaili@sjtu.edu.cn.

†Ph.D. Graduate Student, Institute of Refrigeration and Cryogenic Engineering, 800 Dongchuan Road.

‡Professor, Institute of Refrigeration and Cryogenic Engineering, 800 Dongchuan Road; rswang@sjtu.edu.cn.

I. Introduction

IN GROUND fill applications, the transfer of liquid is straightforward in the presence of vented fills, because vapor can be readily vented as a consequence of the known liquid position. When introduced to applications of dangerous cryogens such as liquefied natural gas and precious liquefied gas such as liquid helium (LHe) and liquid hydrogen (LH_2), vented fills are disadvantageous and substituted by no-vent fills for the sake of safety and resource protection.

Many experimental investigations have been conducted to obtain the feasibility, the characteristics and influencing factors of no-vent fills [1–3]. It reveals that the top filling configurations perform better than the bottom filling ones in the no-vent filling process due to agitation of the ullage/liquid interface and increase of the heat transfer area. Therefore, top filling configurations are more and more popular in no-vent filling applications.

Two common configurations applied in top filling configurations are the spray and the nozzle. Some researchers thought that the top spray is better than the top nozzle, while others thought the top nozzle performs better [4–7]. Performance experiments of both the top-debs-spray and top-nozzle filling configurations were conducted by the authors. Pressure and temperature distribution in the receiver vessels of no-vent fills were systematically studied. The test results showed that the temperature is uniform and equal to the saturated temperature corresponding to the current pressure in the receiver vessels for both top filling configurations, which reveals a thermodynamic saturated equilibrium occurring in the no-vent fill process of the top filling configurations.

However, most models established before were used to predict thermodynamic state during the no-vent filling process for bottom filling configurations, which were used to simulate the worst filling condition in space [8–10]. Little models were reported for top filling configurations. An empirical correlation similar to the submerged jet model of Brown et al. [11] was presented by Vaughan et al. [12], in order to provide a basis for developing a condensation expression that related the top fill to the bottom fill performance. By compared with test data, the expression performed well with liquid height for $Z/D < 1.7$. Above this limit it was not satisfied. Thermodynamic

modeling of the no-vent fill process proposed by Chato [13] and Taylor and Chato [14] referred to the correlation of Brown [15], which was complicated for the heat transfer from droplets of the top spray and neglected the effects of agitation of the ullage/liquid interface.

In this paper, a simple and straightforward TSE (thermodynamic saturated equilibrium) model is established to predict the performance of top filling configurations in no-vent fills. A new method of dealing with heat transfer between the tank wall and the cryogen is introduced to improve the reliability of the simulation. Corrections of the initial distribution of the wall temperature and the inflow rate of the incoming liquid are presented, too. Experiments of both the top-spray and the top-nozzle filling configurations are also conducted in a cryogenic thermal-insulated cylinder with a volume of 180 liters to validate the new model. Pressure, filling by volume, and wall temperature were measured and compared with the results of the TSE model. The model results are shown to match the test results within the measurement uncertainty of the test data.

II. Model Description

The TSE model employs a finite difference analysis scheme that segregates the tank/fluid system into four distinct control volumes on nodes. These include the tank wall in contact with the ullage space, tank wall in contact with the bulk liquid, tank wall in contact with the spray incoming liquid and the cryogen (ullage and bulk liquid as a whole) in the receiver vessel. The mass and energy flows between these regions are calculated at each time step dt. According to the new mass balance and energy distribution, solution of the thermodynamic state variables, such as pressure and temperature are obtained through thermodynamic properties database [16].

A. Mass Balance

During no-vent fills, only the ullage and the liquid regions in the tank undergo variations in mass. The incoming liquid results in a corresponding mass addition to the cryogen remaining in the receiver tank. If the initial pressure in the receiver vessel is less than the saturated pressure of the incoming chunk, a chunk of mass will experiences flash evaporation and it is assumed that the resulting vapor and liquid portions of the chunk are each at their respective saturation conditions according to the current pressure in the receiver vessel. Here, a flashing coefficient is introduced to determine the evaporation capacity of the incoming liquid and defined as follows:

$$\lambda_f = \frac{\dot{m}_f}{\dot{m}_{\text{in}}} = \frac{h_{l\text{in}} - h_{l\text{sat}}}{h_{fg}} \tag{1}$$

Until the pressure in the receiver tank is higher than or equal to the saturated pressure of the incoming liquid, the flash evaporation will be ended. After flash evaporation, the mass of ullage and liquid bulk in the receiver vessel is redistributed as

$$\frac{\mathrm{d}m_g}{\mathrm{d}t} = \lambda_f \times \dot{m}_{\text{in}} \tag{2}$$

$$\frac{\mathrm{d}m_l}{\mathrm{d}t} = (1 - \lambda_f) \times \dot{m}_{\text{in}} \tag{3}$$

If the current pressure in the receiver tank exceeds the saturated pressure of the incoming chunk, the incoming liquid is subcooled with respect to the current tank pressure and $\lambda_f = 0$.

The change in volume for the liquid bulk and the ullage space can now be obtained. Note that the change in volume of the vapor is equal and opposite to the change in volume of the liquid, and the total volume is equal to the tank volume. The volume relationships are

$$\frac{m_g}{\rho_{g\text{sat}}} + \frac{m_l}{\rho_{l\text{sat}}} = V_{\text{tank}} \tag{4}$$

$$m_g + m_l = (m_g + m_l)_{\text{old value}} + \dot{m}_{\text{in}} \tag{5}$$

where $\rho_{g\text{sat}}$ and $\rho_{l\text{sat}}$ are the functions of the saturated temperature, which can be calculated after the current pressure is updated.

B. Energy Balance

The energy balance in the TSE model has been simplified, since the ullage space and the bulk liquid are united as a whole node. In this test system, the total heat leak rate of each receiver cylinder was found out to be lower than 5 W. With test durations ranging from approximately 2.0 to 7.0 min, the total heat leak has a maximum of 2.1 kJ. These small heat leaks are negligible in comparison with the energy of the incoming liquid, and thus do not impact the final pressure in the receiver tank. For the cryogen node, the energy balance includes the energy transported by the incoming liquid and convection with the tank wall:

$$\frac{\mathrm{d}(m_g u_g + m_l u_l)}{\mathrm{d}t} = Q_{\text{hw}g} + Q_{\text{sw}l} + Q_{\text{cw}l} + \frac{\mathrm{d}m_{\text{in}}}{\mathrm{d}t} h_{\text{in}} \tag{6}$$

where $Q_{\text{hw}g}$, $Q_{\text{sw}l}$, and $Q_{\text{cw}l}$ represent heat transfer between the hot tank wall and the ullage space, between the spray region on the tank wall and the incoming liquid, and between the cold tank wall and the bulk liquid, respectively. The model then iterates the tank pressure until the fluid qualities based on the density and internal energy converge. The requisite parameters are then updated and the program proceeds to the next time step.

The convection heat transfer between the tank wall and the cryogen is divided into three regions: 1) between the hot tank wall and the ullage space, 2) between the spray area on the tank wall and the incoming liquid, and 3) between the cold tank wall and the bulk liquid, as shown in Fig. 1. These are composed of $Q_{\text{hw}g}$, $Q_{\text{sw}l}$, and $Q_{\text{cw}l}$. Each region yields the following similar expression for the tank wall adjacent to the liquid:

$$Q_{\text{cw}l} = h_{\text{cw}l} A_{\text{cw}l} (T_{\text{cw}} - T_l) \tag{7}$$

In addition to different T_{wall} and heat transfer areas, three regions correspond to different heat transfer coefficients ($h_{\text{hw}g}$, $h_{\text{sw}l}$, and $h_{\text{cw}l}$) and different corresponding temperatures of the cryogen (T_g, T_f, and T_l).

In the time step of k,

$$Q_{\text{cw}l} = h_{\text{cw}l} \sum_{i=0}^{k} [T_{\text{wall}}(H_i, t_{k-1}) - T_{l,k-1}]\, \mathrm{d}A_i\, \mathrm{d}t \tag{8}$$

where the subscripts i and $k-1$ denote the corresponding time step. For example, H_i is the liquid level at the end of the time step of i. The expression of $T_{\text{wall}}(H_i, t_{k-1})$ indicates the wall temperature at a liquid level of H_i at the beginning of the time step of k. It shows that the wall

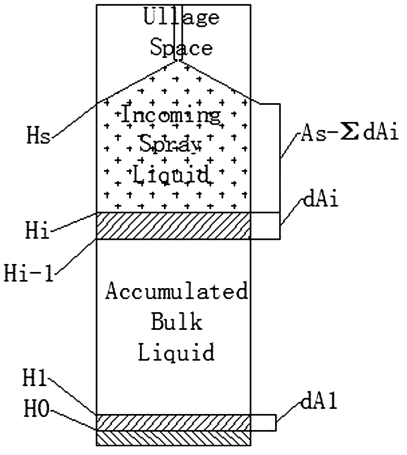

Fig. 1 Schematic of calculation of the heat transfer between the wall and the cryogen.

temperature is a function of both the liquid level and time. The heat transfer between the cold wall and the bulk liquid is solely calculated and then accumulated to give the total rate of the heat transfer of wall/bulk liquid on the assumption that heat conduction along the wall can be omitted.

For region 2 of wall/spray heat transfer,

$$Q_{swl} = h_{swl}[T_{wall}(H_i, H_s, t_{k-1}) - T_f]\left(A_s - \sum_{i=0}^{k} A_i\right) \mathrm{d}t \quad (9)$$

where $T_{wall}(H_i, H_s, t_{k-1})$ is a geometric mean wall temperature in the range of liquid level from H_i to H_s according to the method of lump parameter. Similarly, for region 3 of wall/ullage heat transfer,

$$Q_{hwg} = \begin{cases} h_{hwg}[T_{wall}(H_s, H_{top}, t_{k-1}) - T_g](A_{tank} - A_s)\,\mathrm{d}t & \text{if } H_s \geq H_i \\ h_{hwg}[T_{wall}(H_i, H_{top}, t_{k-1}) - T_g]\left(A_{tank} - \sum_{i=0}^{k} A_i\right)\mathrm{d}t & \text{if } H_s < H_i \end{cases} \quad (10)$$

Meanwhile, the wall temperature at varying liquid level can be calculated with the aid of the division of wall surface by the rising liquid interface in each time step. The relationship between heat transfer on the wall and the heat capacity change of the wall meets

$$\mathrm{d}\,Q_i = h_i\,\mathrm{d}A_i(T_{wall,i-1} - T_{cryogen})\,\mathrm{d}t = M_{wall,i}\,\mathrm{d}(C_{wall,i}T_{wall,i}) \quad (11)$$

where $M_{wall,i} = \rho_{wall}V_{wall,i} = \rho_{wall}D\,\mathrm{d}A_i$. Since h_i, $T_{wall,i-1} - T_{cryogen}$, $\rho_{wall}D$, and $C_{wall,i}$ are known, the wall temperature at varying liquid levels and its history can be obtained.

The division on the tank wall is a new method to be introduced here. Chato [13] once assumed in his no-vent fill (NVFIL) model that no liquid accumulation took place before the tank wall being chilled to the temperature of the incoming liquid and once liquid started to accumulate, the liquid and vapor were in thermodynamic equilibrium. By comparison with the experiment results, the pressure was overestimated, since it was impossible to achieve full heat absorption in the initial filling process. Actually, heat transfer between tank wall and cryogens occurs in every time step, depending on different mechanisms. In this model for top filling configurations, Newton's law of cooling describes the heat convection between the tank wall and cryogens, but it is composed of Q_{hwg}, Q_{swl}, and Q_{cwl}. The model then redistributes new heat transfer area and heat capacity according to the current liquid level and corresponding temperature in each time step to estimate a new heat transfer rate. The heat transfer coefficients (h_{hwg}, h_{swl}, and h_{cwl}) are derived from Sauter et al. [17].

C. Corrections of the Initial Wall Temperature and the Inflow Rate

In most former models [8–14], the wall temperature was assumed as uniform initially and the inflow rate was assumed as a constant for the whole filling process. During practical applications and experiments, it is found that the temperature of the wall in contact with the ullage space changes much and the higher liquid level is the higher wall temperature exists. On the other hand, a constant supply pressure is more easily and economically controlled than a constant inflow rate. In this model, the wall temperature is assumed as a linear function of the liquid level and the inflow rate is a function of the pressure difference between the supply and the receiver pressure.

D. Constitutive Relationships and Model Parameters

At the temperature and pressure of interest, since the specific heat of the liquid, vapor and tank wall is obviously varied, thermal properties database has been involved and the specific heat is assumed as a function of the current temperature in each time step.

In this model, the constant supply pressure is substituted for the constant inflow rate as an input parameter. The inflow rate is a fluid transfer parameter that depends on the flow characteristic of the fluid transfer pipe. It is assumed that the inflow rate is a function of the pressure difference between the supply and the receiver pressure.

For viscid flow, the head loss of a pipe can be expressed as

$$h_{loss} = \frac{\Delta P}{\rho g} = \frac{U^2}{2g} + h_f + h_l \quad (12)$$

where

$$h_f = \lambda\frac{L}{D}\frac{U^2}{2g} \quad (13)$$

is major loss due to friction in the pipe, and

$$h_l = \xi\frac{U^2}{2g} \quad (14)$$

is minor loss due to the components in the pipe system.

The pressure difference can be calculated by using Eqs. (12–14):

$$\Delta P = \frac{\rho}{2}\left(1 + \lambda\frac{L}{D} + \xi\right)U^2 \quad (15)$$

Assuming

$$\gamma = \frac{\rho}{2}\left(1 + \lambda\frac{L}{D} + \xi\right) \quad (16)$$

and mass balance

$$\frac{\mathrm{d}M_{in}}{\mathrm{d}t} = \rho_{in}A_{outlet}U^2 \quad (17)$$

The pressure difference as a function of the inflow rate can be expressed as

$$\Delta P = \frac{\gamma}{(\rho_{in}A_{outlet})2}\left(\frac{\mathrm{d}M_{in}}{\mathrm{d}t}\right)^2 \quad (18)$$

where γ is the characteristic coefficient of the fluid transfer pipe. In this test system, γ of the given fluid transfer pipe is obtained to be 0.01029 as shown in Fig. 2.

The results of the time-step investigation are shown in Fig. 3 on the base of preliminary coefficients and test parameters of the top-spray filling configuration. For a time step greater than about 1 s, the model becomes unstable. A preliminary time step of 0.5 s is selected for model verification. Quasi-equilibrium conditions are assumed for each time step. It is further assumed that all processes for each time step are considered to be isobaric. As such, the saturation conditions remain constant for the duration of the time step. Regardless of the amount of liquid in the tank, the pressure of the vapor is assumed to represent the pressure throughout the tank.

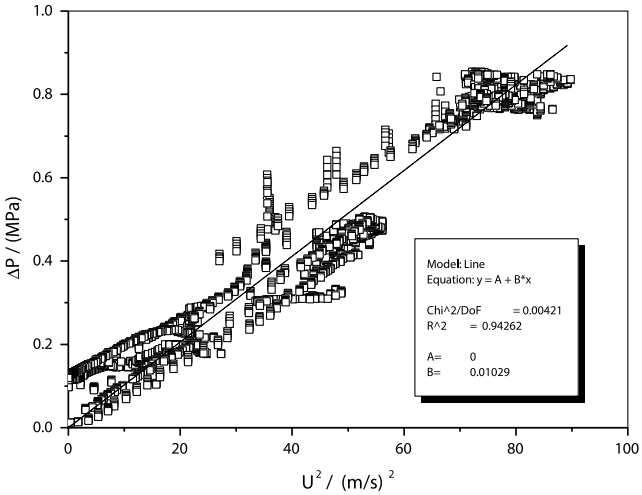

Fig. 2 Transfer characteristic of the given fluid transfer pipe in the test system.

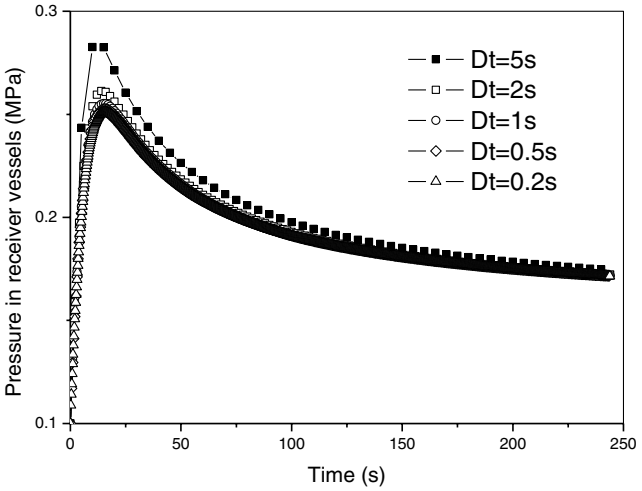

Fig. 3 Time-step study.

Python, a powerful programming language, is used to program the TSE model and nitrogen is served as a work fluid in this system. The thermal properties of nitrogen refer to the thermodynamic properties database [16]. An appropriate set of program stopping conditions are checked at the end of each time step. These checks include the following:

1) The tank pressure exceeds the tank burst pressure or the supply pressure.

2) The fill level is greater than the filling by a volume of 95%.

III. Experiment Description

The test system, illustrated in Fig. 4, comprises the following five parts:

1) The supply system (components 1 and 12) is a vertical supply vessel with a capacity of 5 m^3, in which liquid nitrogen (LN_2) as a testing medium is stored.

2) The LN_2 delivery system (components 3–5) includes a cryogenic pump, a flexible metallic hose, and a bypass pipe line for precooling the pump and the filling line.

3) The receiver system (components 2 and 11) includes a cryogenic thermal-insulated cylinder with a volume of 180 liters.

4) The measuring system (components 6–9) includes temperature sensors positioned on the inner wall and in the inner cylinder,

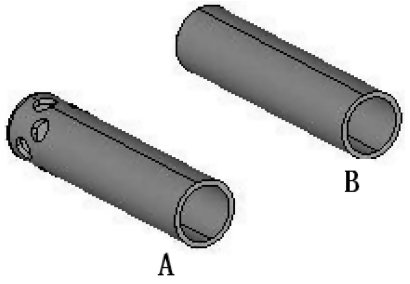

A -spray; B -nozzle

Fig. 5 Sketch of outlets of filling configurations.

pressure transducers on supply and receiver vessels, and weight measurement of the receiver cylinder.

5) The cryogenic safety system (component 10) includes several sets of the burst disc and the safety valves on the transfer pipe line and tanks. LN_2, as the test media, is supplied from the storage vessel and transferred into receivers through the cryogenic pump.

Two patterns including top spray and top nozzle are studied in the no-vent fills. Spray and nozzle outlets are illustrated in Fig. 5. Figure 6 shows out the outlet position of top filling configurations. It is fixed at a relatively higher place that corresponds to a filling by volume of 90%. Figure 6 also illustrates locations of the thermocouples for testing receiver cylinders. Tank wall thermocouples are located in the annular vacuum space and are mounted to the inner tank wall. It contains six thermocouples vertically spaced on the wall. Within the inner cylinder is an instrument tree containing thermocouples at varying heights and radii. This tree is in direct contact with the tank contents, whether liquid or vapor. It contains totally 14 thermocouples assigned to eight layers arranging from 2.7% height level to 95% height level. In addition to the tank wall and tree temperature measurements, one thermocouple is fixed at the outlet of the filling pipe to measure the inflow temperature.

MPM4730 transducers made by Micro Sensor Company provide continuous pressure measurement throughout the system with an accuracy of ± 0.1 percent. The transducers record the ullage pressure of receivers and the outlet pressure of supply vessels. The receiver cylinder is put on the SCS-600 electronic weighing platform made by Mettler Toledo with an accuracy of ± 0.1 kg to estimate the flow rate and filling mass. Temperature measurements are obtained with thermocouples mounted to the inner tank wall and the axial rod at the center of the tank, which is shown in Fig. 6. The thermocouples are calibrated before and after the tests with an accuracy of ± 1 K. With the aid of temperature and mass measurements, liquid or vapor

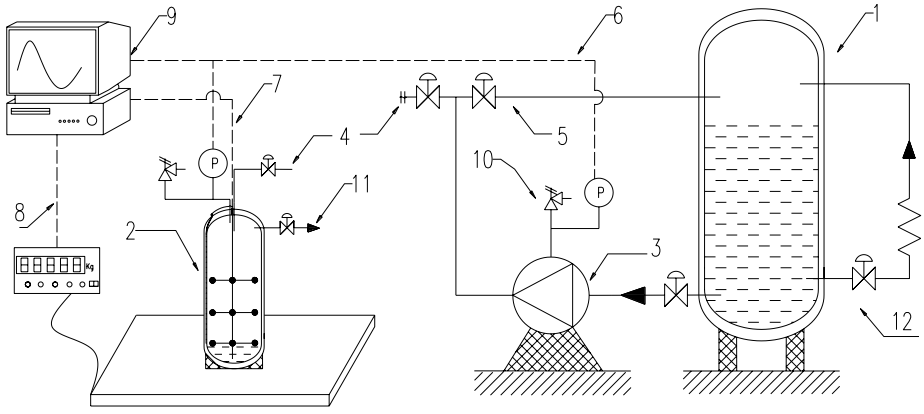

1-supply vessel; 2-180L testing cylinder; 3- cryogenic pump; 4- filling line;5- by-pass precooling pipe line; 6- pressure measurement; 7- temperature measurement; 8- mass measurement; 9–collection system; 10- safety system; 11-vent pipe line; 12-self-pressurizing pipe line.

Fig. 4 Schematic of the filling test loop and measurement system.

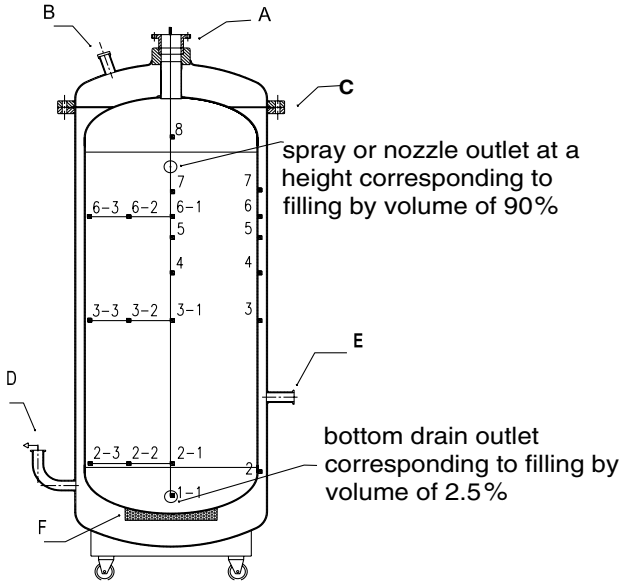

A-exchangeable filling flange; B-aviation joint; C-outer jacket flange;

D-vacuum pipe line; E- vacuum gauge.

Fig. 6 Construction of the receiver tank and position of thermocouples and filling outlets.

density and filling by volume of receiver vessels could be estimated within an error of 4%.

The receiver cylinder selected is a multilayer insulating cryogenic vessel with high vacuum and the annular space is vacuumed to the order of magnitude of 10^{-3} Pa to eliminate the effects of heat convection. To estimate the total heat leak, static evaporation rate measurement is conducted before filling tests to ensure that the total heat leak rate of each receiver cylinder could be omitted.

Precooling is performed for all the receivers and pipes before each fill to avoid abrupt vaporization. Performance of a filling process involves four sequential steps. First, the test cylinders should be chilled down to a target temperature, which is somewhat above the inflow temperature but low enough not to make pressure exceed the allowable maximal value [18]. Second, the cryogenic pump should be chilled down before operating. Third, to eliminate the pressure rise in receivers, the filling pipes should be chilled down until only single-phase LN_2 flows in the filling lines, which could be realized by installing bypass valve at the end of the filling lines. Fourth, when all the preparations have been well done, the filling valve can be open and LN_2 is transferred from the supply vessel to the receiver vessel until the pressure rapidly rises for the second time in the no-vent fills.

IV. Model Validation and Discussion

Test results are used to evaluate the accuracy of the prediction of the TSE model, to check its theoretical and empirical constitutive relationships, and generally validate its use for ground fill analysis. Comparisons between test data and model predictions for both the top-spray and the top-nozzle configurations are shown in Figs. 7 and 8.

Figure 7a shows that the results from the TSE model are in agreement with the test data of the top-nozzle filling configurations, running within 0.05 MPa for most cases. The model underpredicts the initial pressure spike and overpredicts the pressure at the second half of the process. In examining the analytical results, it is noted that although the straight downward direction of the top nozzle leads to assumptions that zero spray area appears on the tank wall and only Q_{hwg} and Q_{cwl} determine the wall/cryogen heat transfer, in a real filling process, the incoming liquid that directly impinges on the bottom surface or the rising liquid/ullage interface causes liquid drops to bounce out to the tank wall, especially at the beginning of the filling process. Such diffusion leads to the increase of heat transfer

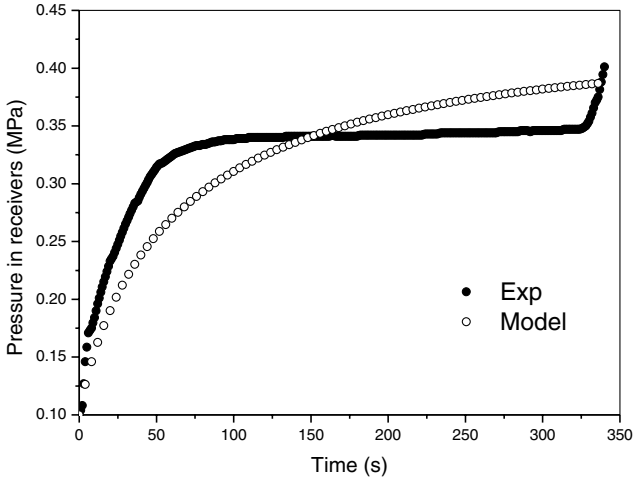

a) Pressure history in the receiver vessel

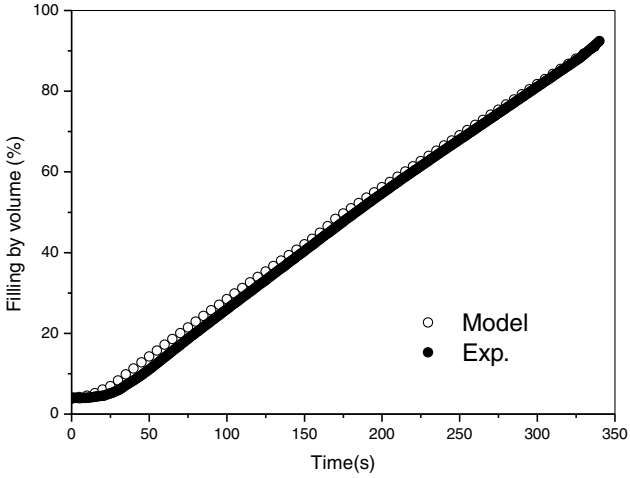

b) Liquid level history in the receiver vessel

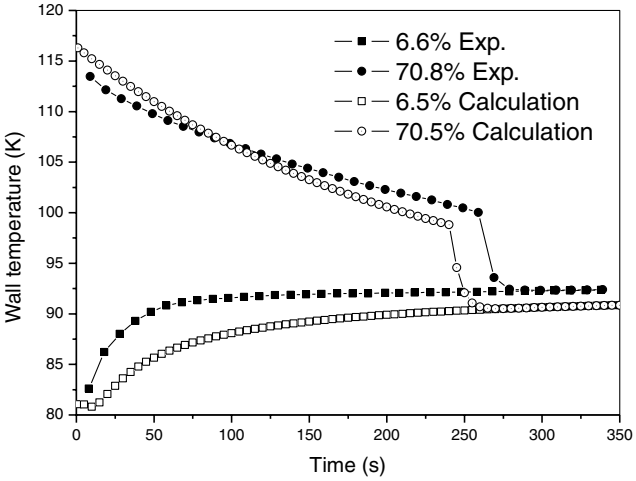

c) Comparisons of the wall temperature

Fig. 7 Comparison of the top-nozzle filling configuration. Test parameters: time step is 0.5 s, $\bar{T}_{\text{in}} = 90.1$ K, $P_{\text{supply}} = 0.65$ MPa, $m_0 = 6.68$ kg, $P_0 = 0.1$ MPa, and $T_{\text{wall}} = 75.73766 + 48.46H$ K.

area and more heat being absorbed to increase the pressure in the receiver tank. As shown in Fig. 7b, the prediction of the filling level is in good agreement with the test results.

The prediction of tank wall temperature is also compared with the test data, which is illustrated in Fig. 7c. The results are shown to

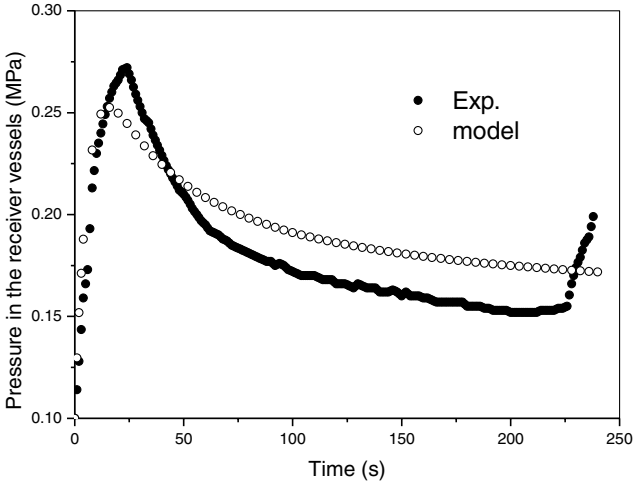

a) Pressure history in the receiver vessel

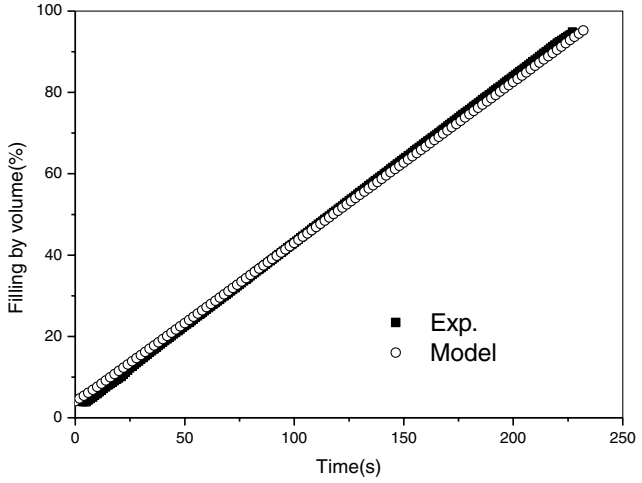

b) Liquid level history in the receiver vessel

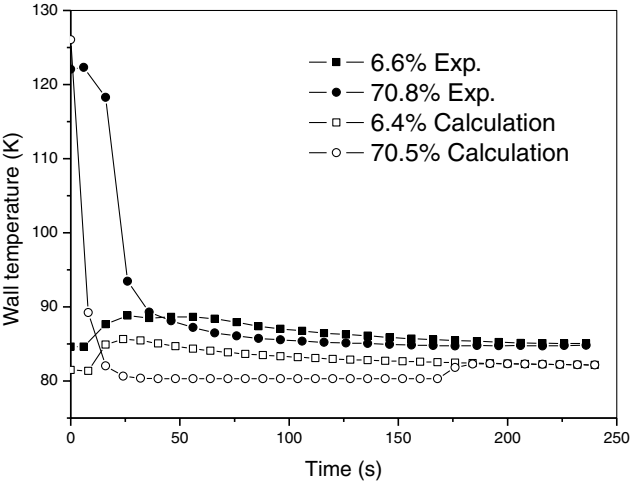

c) Comparisons of the wall temperature

Fig. 8 Comparison of the top-spray filling configuration. Test parameters: time step is 0.5 s, $\bar{T}_{\text{in}} = 80.3$ K, $P_{\text{supply}} = 0.1$ MPa, $m_0 = 6.68$ kg, $P_0 = 0.1$ MPa, and $T_{\text{wall}} = 73.61809 + 61.37H$ K.

match the test results within the measurement uncertainty of the test data. The measured temperature is higher than the calculated one, because the measured nodes are located on the outside surface of the tank wall while the calculated values are for the inner surface of the tank wall. Because of effects of heat conduct and heat radiation from surroundings, the measured temperature is a bit higher than expected one.

The comparisons for the top-spray filling configurations are illustrated in Fig. 8. For the pressure transients, the prediction performs well in Fig. 8a. However, the pressure is still underpredicted at the beginning of the filling process. It can be explained that extra heat leak from the filling transfer line is brought into the receiver tank at the beginning of the filling process, since the transfer line is hard to be totally cooled down in the precooling stage. At the second half of the filling process, the pressure is overpredicted for both the spray and nozzle configurations. It may be caused by the constant assumptions of the heat transfer coefficients between the tank wall and cryogens. Since the temperature difference and flow pattern on the wall/cryogen surface changes, the heat transfer mechanism is naturally transformed from boiling to forced convection. Therefore, the heat transfer coefficients and the equations should be updated to accommodate the practical conditions. As shown in Fig. 8b, the filling level is well predicted by the model.

For test results of both the top filling configurations (Figs. 7a and 8a), in addition to an initial pressure rise region and a relatively moderate pressure stage, there exists another pressure rise at the end of the filling process. It usually happens when the outlets of filling nozzles start to become submerged by the rising liquid/ullage interface. As the outlets are immersed, condensation deceases and the ullage space is compressed. The pressure characteristic of a second pressure rise can be a symbol of terminating the filling process of no-vent fills. Although the pressure rapidly rises after the outlets are submerged, the temperature of the bulk liquid has no change, for the following reasons:

1) When the outlets are submerged, it is hard for the incoming liquid to mix the bulk liquid due to the effects of buoyancy and a large amount of accumulated bulk liquid.

2) The submerged incoming liquid cannot well agitate the rising liquid/ullage interface, which leads to a sharp decrease of heat transfer area and thereby a poor condensation. With poor condensation, less vapor can be liquefied.

3) The continuous incoming liquid occupies the room for the ullage space without escapement or condensation of vapor, which leads to a further compression of the ullage space and thereby a rapid pressure rise.

The phenomenon of a rapid pressure rise with subcooled bulk liquid at the end of no-vent filling process has been observed in experiments. It is clear that the model becomes inappropriate after the outlets are submerged, since the cryogen in the receiver tank is not in accord with the assumption of thermal saturated equilibrium. It shows that the TSE model should be refined for the state after outlets submerged.

Two assumptions on the initial wall temperature and the inflow rate have been corrected in this model and their effects have been

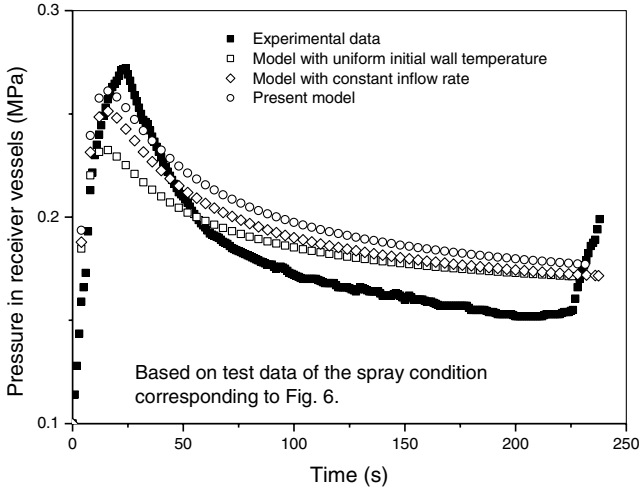

Fig. 9 Model comparison among different assumptions.

shown in Fig. 9. The results from the current model are in much better agreement with the test data, since the new assumptions obey the actual distribution of the tank wall temperature and the transfer characteristics of the filling pipe. The constant assumption of the initial wall temperature performs worst as shown in Fig. 9, which indicates that the initial wall temperature is an important influencing factor to which attention should be paid.

V. Conclusions

A thermodynamic saturated equilibrium analytical model to estimate no-vent fill performance of the top filling configurations has been established. The validity of the model is demonstrated by a series of experimental tests. The results are in good agreement with the test data of top filling configurations. The corrections of assumptions on the initial wall temperature and the inflow rate are effective to improve the model's accuracy.

The continuing refinement of the current model will lead to a general program that can be applied to all kinds of filling configurations and vessels for a 1 *g* environment. Some areas currently under consideration for refinement include better simulation of heat transfer rate between tank wall and cryogen, the applications of jet-submerged theory for submergence conditions, and the addition of external heat leak effects.

Acknowledgments

The support of the Cryogenic Engineering Group of the Institute of Refrigeration and Cryogenic Engineering of Shanghai Jiaotong University of China is greatly appreciated.

References

[1] Chato, D. J. , "Cryogenic Transfer Options for Exploration Missions," AIAA Paper 91-3541, 1991.

[2] Chato, D. J. , and Taylor, W. J., "Small Experiments for the Maturation of Orbital Cryogenic Transfer Technologies," NASA TM-105849, 1992.

[3] Taylor, W. J., Chato, D. J., Moran, M. M., and Nyland, T. W., "On-Orbit Cryogenic Fluid Transfer Research at NASA Lewis Research Center," *Cryogenics*, Vol. 32, No. 2, 1992, pp. 199–204. doi:10.1016/0011-2275(92)90267-E

[4] Moran, M. E., Nyland, T. W., and Driscoll, S. L., "Hydrogen No-Vent Fill Testing in a 1.2 Cubic Foot (34 Liter) Tank," NASA TM-105273, 1991.

[5] Schmidt, G. R., Carrigan, R. W., Hahs, J. E., Vaughan, D. A., and Foust, D. C., "No-vent Fill Pressurization Tests Using a Cryogen Simulant," NASA TM-103561, 1992.

[6] Moran, M. E., and Nyland, T. W., "Hydrogen No-Vent Fill Testing in a 5 Cubic Foot (142 Liter) Using Spray Nozzle and Spray Bar Liquid Injection," *28th AIAA/SAE/ASME/ASEE, Joint Propulsion Conference and Exhibit*, Nashville, TN, 1992.

[7] Wang, C. L., Wang, R. S., Li, Y., Xie, G. F., and Chang, C., "Comparison of the Performance About 4 Different Filling Configurations in No-Vent Fill Processes," *Cryogenics*, Vol. 165, No. 5, 2008, pp. 35–39 (in Chinese).

[8] Gille, J. P., "Analysis and Modeling of No-Vent Transfer of Cryogens in Orbit," *4th AIAA/ASME Joint Thermophysics and Heat Transfer Conference*, Boston, 1986.

[9] Vaughan, D. A., and Schmidt, G. R., "Analytical Modeling of No-Vent Fill Process," *Journal of Spacecraft and Rockets*, Vol. 28, No. 5, 1991, pp. 574–579. doi:10.2514/3.26283

[10] Fite, L. W., "Characteristics of Nonvented Propellant Transfer," Ph.D. Dissertation, Memphis State Univ., Memphis, TN, 1993.

[11] Brown, J., Hemlick, M., and Sonin, A., "Vapor Condensation at a Turbulent Liquid Surface in Systems with Possible Space-based Application," AIAA Paper 89-2846, 1989.

[12] Vaughan, D. A., Foust, D. C., and Schmidt, G. R., "Enhancement of the No-Vent Fill Process," *27th SAE/ASME/ASEE Joint Propulsion Conference*, Sacramento, CA, 1991.

[13] Chato, D. J., "Analysis of the Nonvented Fill of a 4.96 Cubic Meter Lightweight Liquid Hydrogen Tank," *ASME/AIChE National Heat Transfer Conference*, Philadelphia, 1989.

[14] Taylor, W. J., and Chato, D. J., "Improved Thermodynamic Modelling of the No-Vent Fill Process and Correlation with Experimental Data," 26th AIAA Thermophysics Conference, Honolulu, AIAA Paper 91-1379, 1991.

[15] Brown, G., "Heat Transfer by Spray Cooling," *IME and ASME General Discussion on Heat Transfer*, London, 1951, pp. 49–52.

[16] Jacobsen, R. T., Penoncello, S. G., and Lemmon, E. W., *Thermodynamic Properties of Cryogenic Fluids*, Plenum, New York, 1997, Chap. 5.

[17] Sauter, D. R., Hochstein, J. I., and Fite, L. W., "Computational Modeling of Cryogenic Propellant Resupply," 44th AIAA Aerospace Sciences Meeting and Exhibit, Reno, NV, AIAA Paper 2006-984, 2006.

[18] DeFelice, D. M., and Aydelott, J. C., "Thermodynamic Analysis and Subscale Modeling of Space-Based Orbit Transfer Vehicle Cryogenic Propellant Resupply," AIAA Paper 87-1764, 1987.